Evaluation of Self-Magnetically Pinched Diodes up to 10 MV as High-Resolution Flash X-Ray Sources

Stephen B. Swanekamp, Gerald Cooperstein, Joseph W. Schumer, David Mosher, F. C. Young, Paul F. Ottinger, *Senior Member, IEEE*, and Robert J. Commisso

***Abstract*—The merits of several high-resolution, pulsed-power-driven, flash X-ray sources are examined with numerical simulation for voltages up to 10 MV. The charged particle dynamics in these self-magnetically pinched diodes (SMPDs), as well as electron scattering and energy loss in the high-atomic-number target, are treated with the partic by coupling the output from LSP with the two-dimensional component of the integrated tiger series of Monte Carlo electron/photon transport codes, CYLTRAN. The LSP/CYLTRAN model agrees well with angular dose-rate measurements from positive-polarity rod-pinch-diode experiments, where peak voltages ranged from 5.2–6.3 MV. This analysis indicates that, in this voltage range, the dose increases with angle and is a maximum in the direction headed back into the generator. This suggests that high-voltage rod-pinch experiments should be performed in negative polarity to maximize the extracted dose. The benchmarked LSP/CYLTRAN model is then used to examine three attractive negative-polarity diode geometry concepts as possible high-resolution radiography sources for voltages up to 10 MV. For a 2-mm-diameter reentrant rod-pinch diode (RPD), a forward-directed dose of 740 rad(LiF) at 1 m in a 50-ns full-width at half-maximum radiation pulse is predicted. For a 2-mm-diameter nonreentrant RPD, a forward-directed dose of 1270 rad(LiF) is predicted. For both RPDs, the on-axis X-ray spot size is comparable to the rod diameter. A self-similar hydrodynamic model for rod expansion indicates that spot-size growth from hydrodynamic effects should be minimal. For the planar SMPD, a forward-directed dose of 1370 rad(LiF) and a similar X-ray spot size are predicted. These results show that the nonreentrant RPD and the planar SMPD are very attractive candidates for negative-polarity high-resolution X-ray sources for voltages of up to 10 MV.**

***Index Terms*—Bremsstrahlung, coupled electron–photon transport, electron beams, flash X-radiography, high-power diodes, ion beams, Monte Carlo, particle-in-cell.**

I. Introduction

INTEREST in pulsed-power-driven flash radiography is currently being fueled by the desire to radiograph dense objects that are rapidly accelerated by high explosives [1]. The characteristics of the radiographic system are dictated by properties of the object to be radiographed including the spatial scale of the features to be resolved, the high-speed motion, and the areal density. Because the object is moving rapidly (several kilometers per second), a flash X-ray source of duration no longer than 50-ns full-width at half-maximum (FWHM) is desired to minimize motion blur in the image. In addition, the areal density of the object is equivalent to tens of cm of lead and so that a large flux of 3–5-MeV photons is required to penetrate the object and still produce a measurable signal at the detector. An accelerating voltage of 10–15 MV is required to produce a significant flux of these photons. Information theory has been applied to determine the dose and spot-size requirements that are necessary to obtain high-quality images [1]. This analysis indicates that a dose of 1000 rad(air) at a distance of one meter from a 2-mm-diameter, uniformly radiating disk will produce images of sufficient quality. Unless otherwise noted, doses in the remainder of this article are quoted at one meter from the source with equilibrated lithium-fluoride (LiF) detectors. The spectral differences in the responses of air and LiF dosimeters are negligible over the range of photon energies of interest.

Currently, the only sources that approach these requirements are produced with linear induction accelerators (LIA) [2]. These machines are currently capable of producing doses of many hundreds of rads in a 2-mm-diameter uniform disk for a duration of approximately 50 ns. Because LIAs are many times more expensive than an equivalent pulsed-power machine, the Atomic Weapons Establishment (AWE), Aldermaston, U.K., has chosen a magnetically insulated, inductive-voltage adder (IVA) technology for their Hydrodynamic Research Facility (HRF). The design parameters for the IVA currently envisioned for the HRF are 14 MV and 140 kA [3]. One of the biggest challenges with pulsed-power-driven radiography is to demonstrate that both the dose and spot-size goals can be achieved at these voltage and current levels.

Pulsed-power-driven radiographic source development is currently being pursued with three different types of electron-beam diodes. The immersed-B diode uses an external 10–50-T magnetic field to guide electrons emitted from a millimeter-sized cathode needle onto a high-atomic-number (high-Z) target where an intense X-ray source is formed [4]–[6]. In the paraxial diode, electrons are electrostatically accelerated onto and through a thin, low-mass anode foil. After exiting the foil, the beam enters a gas-filled focusing cell where conductivity generated by the interaction of the beam with the gas in the cell provides space charge and current neutralization. When the beam current and space charge are completely neutralized, the electron beam focuses ballistically onto a high-Z target

Manuscript received December 16, 2003; revised February 11, 2004. This work was supported in part by the U.S. Department of Energy through Sandia National Laboratories and in part by the Atomic Weapons Establishment, Aldermaston, U.K.

S. B. Swanekamp, D. Mosher, and F. C. Young are with the Plasma Physics Division, Naval Research Laboratory, Washington, DC 20375 USA, and also with Titan/Jaycor, Inc., McLean, VA 22102 USA (e-mail: swane@calvin.nrl.navy.mil).

G. Cooperstein, J. W. Schumer, P. F. Ottinger, and R. J. Commisso are with the Plasma Physics Division, Naval Research Laboratory, Washington, DC 20375 USA.

Digital Object Identifier 10.1109/TPS.2004.835956

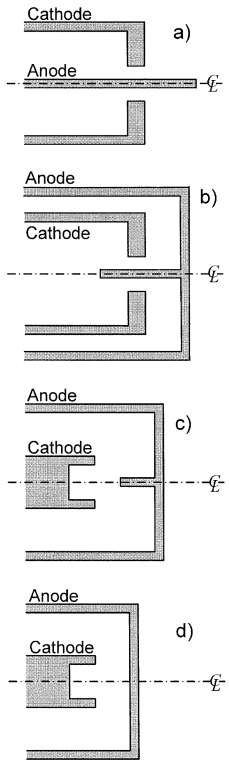

Fig. 1. Diode geometries for high-resolution flash X-ray sources. (a) Positive-polarity reentrant RPD. (b) Negative-polarity reentrant RPD. (c) Negative-polarity nonreentrant RPD. (d) Negative-polarity planar SMPD.

where a small diameter X-rays source is formed [7]–[11]. The third type of diode being developed relies on the self-generated magnetic field of the electron beam to focus electrons onto a high-Z target. Diodes in this category are the subject of the present article and include the rod-pinch diode [12]–[17] (RPD) and the planar self-magnetically pinched diode (SMPD) [18]. Since self-pinched diodes rely on a strong self-magnetic field, they typically operate with two-to-three times lower impedance ($\sim 50\ \Omega$) than the immersed-B or paraxial diodes. The present IVA design for the HRF has the flexibility to be converted to lower impedance to drive either a RPD or a SMPD [3]. In this mode, the IVA will operate at about 10 MV and 200 kA.

The positive polarity version of the RPD is shown in Fig. 1(a). It consists of a small diameter, blunt or tapered, high-Z anode rod that protrudes a few centimeters beyond a thin annular cathode. When the rod is tapered, the last 10-mm portion of the rod that extends beyond the cathode is tapered down to a point. Experiments and simulations show that tapering the anode rod has little effect on the diode impedance but considerably reduces the observed X-ray source size. This geometry will be referred to as "reentrant" because the anode rod extends through the annular cathode. The electron spatial distribution from a PIC simulation of a positive-polarity, reentrant RPD with a tapered anode rod is shown in Fig. 2. The strong self-magnetic field, along with ion emission from the rod, guides and focuses the electron beam onto the end of the rod. An intense X-ray source is formed at the rod tip with a spot size comparable to the diameter of the rod when viewed along the axis of the rod. [15] Recent RPD experiments on the ASTERIX generator at

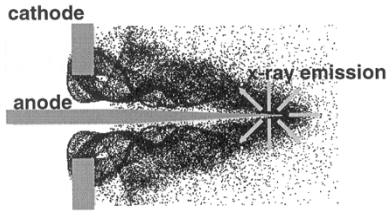

Fig. 2. Electron positions from a particle-in-cell simulation of the positive-polarity reentrant RPD with a tapered anode rod.

the Centre d'Etudes de Gramat (CEG) in France have produced 35 rad(air) at 6 MV in a 2-mm-diameter spot [19], [20]. The uniformly filled-circle definition of spot size developed by AWE is used throughout this article [8].

The ASTERIX results and related numerical simulations indicate that the angular dose distribution from a RPD is peaked in the backward direction and most of the radiation in positive polarity is headed toward the generator along the length of the rod [21]. This suggests that high-voltage RPD experiments should be performed in negative polarity to maximize the extracted dose [22]. One such negative-polarity geometry is the reentrant geometry shown in Fig. 1(b). This geometry is topologically similar Fig. 1(a) but configured to be driven in negative polarity. A second negative-polarity RPD geometry considered in this article is the nonreentrant RPD in which the anode rod does not protrude through the plane of the cathode as shown in Fig. 1(c). The length of the rod can be much shorter in this geometry reducing both the ion-current fraction and the absorption of photons as they pass through the rod. However, the electrostatic fields in this geometry are lower than in the reentrant geometry which reduces the SCL current. This makes it more difficult to obtain self-magnetic fields that are large enough to obtain a tightly pinched electron beam. A final negative-polarity geometry considered in this article is the planar SMPD which consists of a hollow cylindrical cathode and a high-Z planar target, as shown Fig. 1(d). Electrons accelerated from the hollow cathode are pinched by the self-magnetic field onto the planar anode to form a small spot-size X-ray source. Recent SMPD experiments at 4.2 MV have demonstrated 65 rad in a 2.8-mm-diameter X-ray spot [18].

The remainder of this article presents a comparison of the on-axis X-ray dose and spot size obtained from numerical simulations of the four diode geometries depicted in Fig. 1. The analysis is performed by coupling the output from the PIC code LSP [23], [24], which is used to simulate the charged particle dynamics in the diode, to the integrated tiger series [25] (ITS) of electron/photon transport codes, which is used to compute the radiation field. A brief discussion of the physics of SMPDs is presented in Section II. Detailed comparisons between the numerical simulations and recent angular-dose measurements from positive-polarity RPD experiments on ASTERIX are also presented in Section II. In Section III, the LSP/CYLTRAN model that is benchmarked in Section II is used to evaluate the relative merits of the four geometries depicted in Fig. 1 as high-voltage, high-resolution radiography sources. Some practical considerations are discussed in Section IV. The conclusions of the article are presented in Section V.

II. Radiation Calculations for Positive-Polarity Reentrant Rod-Pinch Diodes

A full discussion of the RPD physics is given elsewhere [13], [14]. A small portion of that work is repeated here to allow the reader to more easily follow the discussions of each diode. The electron flow in a RPD can be divided into three regimes. A low-voltage, low-current regime characterized by space-charge-limited (SCL) flow, a high-voltage, high-current regime characterized by strongly pinched, magnetically limited (ML) flow, and an intermediate regime where the flow is weakly pinched [13].

A. SCL Regime

When the voltage is low, the current is too small to generate a sizable self-magnetic field and the electron flow in the diode is SCL. In this regime, electrons flow perpendicular to equipotential lines and are spread out over a large area of the anode. The nonrelativistic form for the single-species SCL current appropriate for cylindrical diodes was first derived by Langmuir and Blodgett [26] and is given by

$$I_{\rm LB} = I_\alpha \frac{2\sqrt{2}}{9}\frac{L_{\rm eff}}{{\rm r_A}\kappa^2}U_0^{3/2} \approx 5.36\frac{L_{\rm eff}}{{\rm r_A}\kappa^2}U_0^{3/2}\ {\rm kA} \qquad (1)$$

where $I_\alpha = {\rm m_e c^3/e} (\approx 17\ {\rm kA})$, $U_0 = {\rm eV/m_e c^2}$ is the diode voltage V normalized to the electron rest mass energy, e is the magnitude of the electron charge, $\rm m_e$ is the electron rest mass, c is the speed of light in vacuum, $L_{\rm eff}$ is the effective cathode length, and κ can be expressed in a power series in $\ln({\rm r_C/r_A})$ where $\rm r_C$ and $\rm r_A$ represent the cathode and anode radii. Since (1) does not include two-dimensional (2-D) effects, the effective diode length $L_{\rm eff}$ is larger than the physical length of the cathode and takes into account the spreading of current as electrons approach the anode. Empirically, it has been found that this effective length can be approximated by $L_{\rm eff} = L_{\rm C} + 2D$, where $L_{\rm C}$ is the length of the cathode and $D = {\rm r_C} - {\rm r_A}$ is the A-K gap spacing. The additional factor of $2D$ accounts for an approximate 45° spreading of the electrons upstream and downstream of the cathode.

The emission of ions from the anode is also important for high-power RPDs. The presence of ions allows for an increase in the electron SCL current. The electron current in bipolar cylindrical diodes increases by a factor of 1.86 for ${\rm r_C/r_A} \sim 1$ (i.e., planar geometry) [27] and by a factor of to 5.5 for ${\rm r_C/r_A} = 60$ over the single-species SCL current. [14] To maintain the impedance range appropriate for radiography sources, ${\rm r_C/r_A} \sim 11$ where the electron current increases by a factor of 3.1. This is sufficient to allow the electron flow to enter the ML regime for voltages above 1 MV.

B. Magnetically Limited Regime

At sufficiently high voltage, the current is large enough to generate a self-magnetic field that limits the current. To enter this regime, the diode must first draw enough SCL current to exceed critical current. In the ML regime, electrons $\mathbf{E} \times \mathbf{B}$ drift along equipotential lines and cross to the anode in a region where the magnetic field is small. The rapid propagation of electron flow down the rod requires ion emission along the length of the rod which produces a concentration of the electron beam at the rod tip.

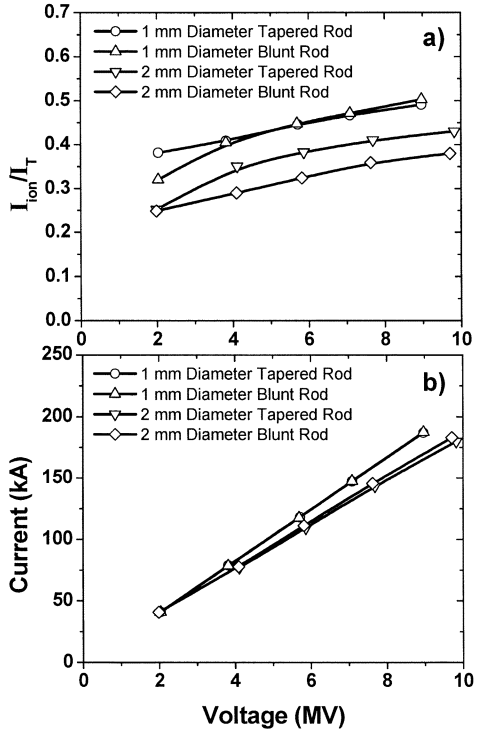

Fig. 3. (a) Proton-current fraction and (b) the total current from PIC simulations of positive-polarity, reentrant, RPDs with 1- and 2-mm-diameter blunt and tapered anode rods.

The form of critical current appropriate for the RPD geometry is given by [13]

$$I_{\rm crit}({\rm kA}) = \frac{8.5\alpha(\gamma^2-1)^{1/2}}{\ln(\frac{\rm r_C}{\rm r_A})} \qquad (2)$$

where $\gamma = 1 + {\rm eV/mc^2}$ is the relativistic factor. Recent research shows that α depends on ion space-charge, electron kinetics, and 2-D effects [28]–[30]. PIC simulations show that the α factor is also sensitive to the position from which ion emission is enabled along the anode [31]. Proton emission from the anode rod is allowed in the simulations from a position extending from one A-K gap upstream of the cathode aperture to the end of the rod. With this assumption, PIC simulations show that α varies from 2.1 to 2.8 as the aspect ratio $({\rm r_C/r_A})$ varies from 1 to 20 [14]. A comparison of the total current from LSP simulations of 1- and 2-mm-diameter tapered and blunt tungsten rods is shown in Fig. 3(b). This figure shows that the diode current depends only on the geometry in the vicinity of the anode-cathode (A-K) gap and does not depend on the rod-tip geometry. The α factor is 2.75 for the 1-mm-diameter rods and is 2.55 for the 2-mm-diameter rods. These α factors are consistent with those previously published that did not include electron scattering in the anode rod [14].

Ion currents in the ML regime are enhanced over the bipolar value due to the increased electron path-length in the diode as their orbits are influenced by the self-magnetic field [32], [33]. Since the electron and ion space charges must be approximately equal, the increased electron path length in the ML regime leads

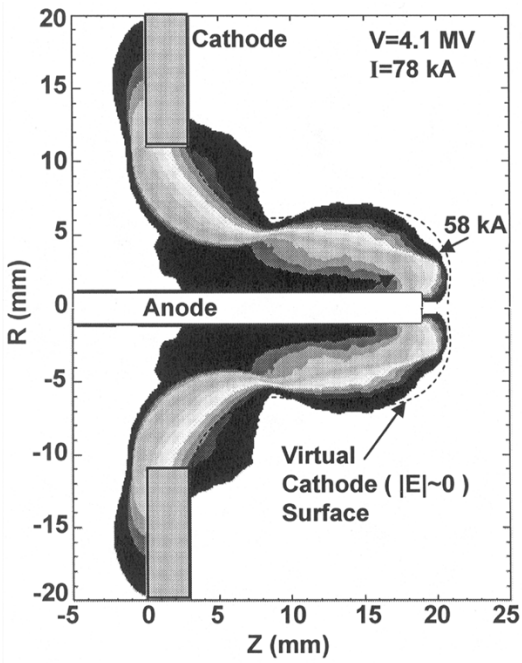

Fig. 4. Current flow pattern from a PIC simulation of the positive-polarity, reentrant, RPD with a 2-mm-diameter blunt anode rod.

to an enhancement in the ion current over the bipolar value. This enhancement is proportional to the ratio of the electron and ion path lengths. For the reentrant RPD, electrons travel the length of the rod while ions travel across the A-K gap so that the ion-current enhancement is about $(1 + L_{\rm rod}/D)$ [14]. For large-aspect-ratio diodes with $L_{\rm rod} \gg D$, the ion current can be a large fraction of the total diode current.

Experiments have shown protons to be the dominant species in these diodes [34] so protons are taken to be the ion species in the simulations presented in this article. The proton-current fractions from LSP simulations of the positive-polarity reentrant RPD with 1- and 2-mm-diameter tapered and blunt tungsten anode rods and voltages between 2 and 10 MV are shown in Fig. 3(a). The proton current is 25%–35% of the total current at 2 MV and increases slowly with voltage to about 40%–50% at 10 MV. In a magnetically limited diode, it is the total current that is limited (i.e., $I_T = I_{\rm crit}$). Therefore, ions reduce the number of electrons that to flow to the rod tip and, since ions do not make X-rays, they represent inefficiency in RPD and SMPD sources. X-ray output can be increased by reducing ion currents. Negative-polarity geometries that significantly reduce the ion-current fraction will be examined in Section III.

Contours of constant rB_θ for a 2-mm-diameter blunt reentrant RPD at 4 MV are shown in Fig. 4. The direction of current flow is parallel to the contours and there are equal amounts of current between adjacent contours. Twenty equally spaced contour levels are used in all the contour plots presented in this article. Also shown is the position of the virtual cathode ($|\mathrm{E}| \sim 0$) defined by the contour where the electric-field magnitude has dropped by two orders of magnitude compared with the average field in the A-K gap. The electrons $\mathbf{E} \times \mathbf{B}$ drift down the rod along the virtual-cathode contour and cross to the anode near the tip of the rod. Particle plots (not shown) indicate that proton emission is distributed over the entire portion of the rod that extends beyond the cathode while electrons connect with the rod only over the last 3–5 mm. Therefore, the current that connects with the last 3–5 mm of the rod is primarily from electrons. A significant fraction of the current flow is also bent around the end of the rod and enters the rod perpendicular to the end. Side viewing X-ray images from the ASTERIX experiments also indicate that a significant fraction of the electrons are concentrated on the end face of the blunt rod [35]. The flow pattern shown in Fig. 4 is representative of the flow patterns in the ML regime at higher voltages.

C. Analysis of ASTERIX Angular Dose-Rate Measurements

The angular distribution of the radiation from a RPD is calculated with a combination of LSP and ITS. The approach is similar to that used to calculate the forward-directed (0°) dose for voltages up to 4 MV [24]. First, LSP is used to model the complex electron and ion dynamics in the diode for a number of steady-state voltages. Included in these calculations are interactions of the electrons with the tungsten anode rod. Electron interactions in the tungsten rod are followed in LSP by incorporating electron scattering, energy loss, and bremsstrahlung production algorithms from ITS. The relevant electron interactions in the rod include collisional energy loss to ionization and excitation, the production of bremsstrahlung, and K-shell and L-shell ionization events that produce characteristic X-ray fluorescence lines and Auger electrons. The tungsten rod used in the LSP simulations protrudes through a hole in the cathode and extends 16 mm beyond the plane of the cathode. The cathode length (L) is 3 mm and, to achieve the impedance range of interest, the cathode diameter is changed in proportion to anode diameter to maintain a constant aspect ratio of $\mathrm{r_C/r_A} = 11$. Once a steady-state voltage is achieved, a list of electron positions and momenta incident on the surface of the high-Z anode rod is generated. The electron list is post processed with the ITS code CYLTRAN to calculate the angular distribution of the radiation spectrum emerging from the rod. A second method of calculating the radiation spectrum utilizes the capability of LSP to generate a list of photons that contains their energy, direction, and location in the rod as they are created. The angular distribution of the radiation spectrum can then calculated by using CYLTRAN to model self absorption in the rod. The relevant photon interactions followed by ITS include Compton scattering, photoelectric absorption, and pair production. The two methods provide an excellent cross check and both methods produce essentially the same results.

The angular dose distribution is calculated from the radiation spectrum using

$$\frac{\mathrm{Dose}(\theta)}{\mathrm{Q_e}} = \int_0^\infty \rho(h\nu) F(h\nu) \frac{d\Phi(\theta, h\nu)}{d(h\nu)} d(h\nu) \qquad (3)$$

where $\mathrm{Q_e}$ is the incident electron charge on the rod, $\rho(h\nu)$ is the spectral response of the detector [dose per photon flux], $F(h\nu)$ is the attenuation by filters between the source and the detector, and $d\Phi/d(h\nu)$ is the angular distribution of the photon flux spectrum at the detector per incident electron charge calculated from the coupled LSP/CYLTRAN simulations. The

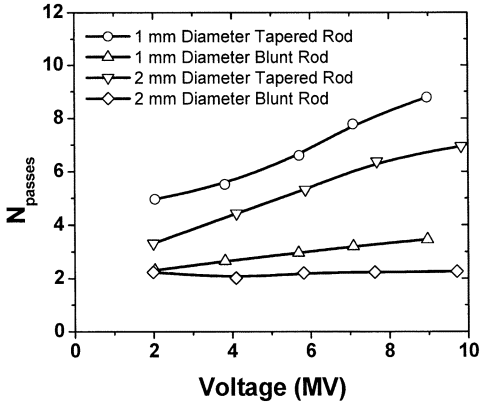

Fig. 5. Number of passes electrons make in 1- and 2-mm-diameter blunt and tapered tungsten anode rods from PIC simulations of the positive-polarity, reentrant, RPD.

CYLTRAN simulations are divided into 18 angular bins so that photon statistics are collected and averaged over 10° bins. The forward-directed angular bin is defined to be $0° \leq \theta < 10°$ and the backward-directed bin is $170° \leq \theta < 180°$. Both the detector response and the filter attenuation are calculated using tabulated attenuation/absorption coefficients [36]. This approach avoids the problem of poor photon counting statistics associated with the small solid angle subtended by the detectors incurred with direct modeling of the detectors with ITS. However, (3) omits radiation scattered in the filters that can subsequently reach the detector. It can also overestimate the energy absorbed in the detector if it is not properly equilibrated. Both of these effects are small in this experiment and the forward dose predicted by (3) agrees with that calculated in [24], where the detectors are modeled directly with ITS.

To compare with experimental results, the incident electron charge on the rod in (3) must be related to at least one measurable quantity. This is accomplished by

$$\mathrm{Q_e} = \mathrm{Q}_T N_{\mathrm{passes}} \left(\frac{1 - I_{\mathrm{ion}}}{I_T} \right) \tag{4}$$

where Q_T is the total charge transferred in the diode (i.e., the integral of the diode current including both electron and ion current), N_{passes} is the number of passes the electrons make in the high-Z target, defined as the ratio of incident electron charge to absorbed electron charge, and I_{ion}/I_T is the ion-current fraction. The quantities Q_T and I_{ion}/I_T are obtained from LSP (see Fig. 3), and N_{passes} can be obtained from either CYLTRAN or LSP. To apply (3) to time-dependent experiments, (4) is used to eliminate $\mathrm{Q_e}$ and the dose-per-charge is interpreted as the dose rate divided by the total current so that

$$\frac{\mathrm{Dose}}{\mathrm{Q}_T} = \frac{\dot{D}}{I_T} \tag{5}$$

where $\dot{D}$ is the dose rate and I_T is the total diode current. This relationship assumes that the charged-particle flow in the diode remains in a quasi steady state at all times.

N_{passes} for 1- and 2-mm-diameter tapered and blunt rods are shown in Fig. 5. It is important to note that a backscattered electron is indistinguishable from an electron that passes through the rod. This is why $N_{\mathrm{passes}} > 1$ at low voltages where the rod diameter is large compared with the electron continuously slowing-down-approximation (CSDA) range. For blunt rods, electrons make two-to-four passes through the rod and N_{passes} is nearly independent of voltage. For tapered rods, N_{passes} is larger and increases with voltage primarily due to electrons reflexing through the rod tip.

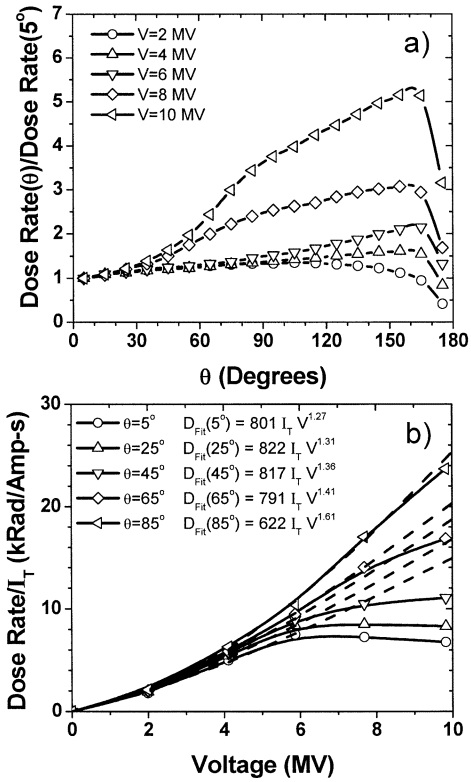

Fig. 6. (a) Angular variation of the dose rate and (b) the dose-rate efficiencies from coupled LSP/CYLTRAN simulations of the positive-polarity, reentrant RPD with a 2-mm-diameter tapered anode rod.

Results from angular dose calculations for a 2-mm-diameter tapered rod are shown in Fig. 6. The values of θ in Fig. 6 are the centers of the angular bins and the data points are average dose rates obtained from photons collected $\pm 5°$ around the centers of the bins. Fig. 6(a) shows that the dose rate is nearly independent of angle for voltages below 4 MV. At higher voltages, the dose rate increases monotonically with polar angle except near 180° where it decreases sharply due to photon self-absorption in the rod. The simulations predict that the dose rate at 6 MV is more than a factor of two larger at 165° than at 5°. This result suggests that, to maximize the extracted dose, RPD experiments at or above 6 MV should be performed in negative polarity [22]. In addition, steps should be taken to minimize photon absorption in the rod by using low-Z, low-mass supporting materials. Fig. 6(b) shows the dose-rate efficiency ($\dot{D}/I_T$) as a function of voltage for several angles. The forward-directed dose-rate efficiency becomes insensitive to changes in the voltage for voltages above 6 MV. This insensitivity and the peaking of the dose rate at large angles is due to electron angles of incidence on the rod approaching 180° at high voltage which increases the X-ray emission at large angles relative to smaller angles. Power-law fits to the dose rates at various angles of the form $A\,I\,V^m$ are

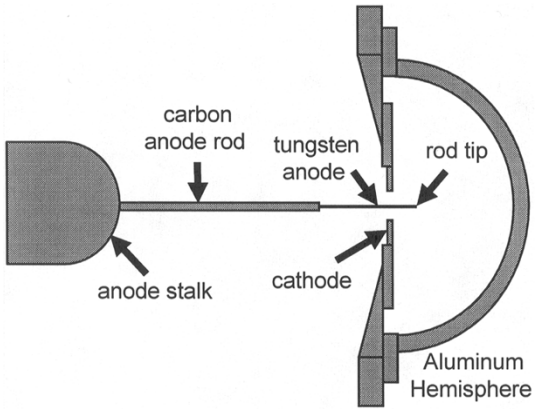

Fig. 7. Schematic of the positive-polarity, reentrant, rod-pinch-diode geometry used in the ASTERIX experiment.

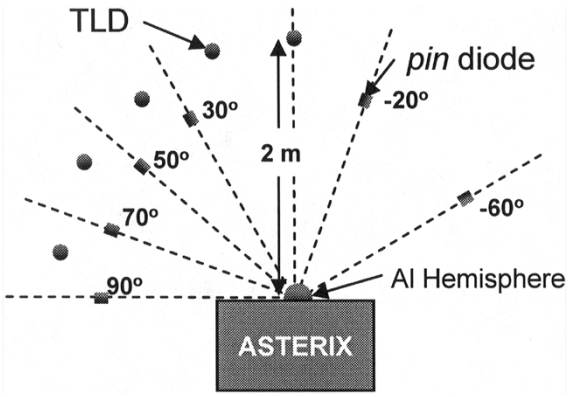

Fig. 8. Schematic showing the locations of the pin diodes and TLDs used in the ASTERIX experiments.

also shown in Fig. 6(b). These fits are valid for voltages up to 6 MV and are used in analyzing the ASTERIX angular dose measurements where peak voltages ranged from 5.2–6.3 MV.

For the ASTERIX experiments, [19]–[21] tungsten or gold anode rods of 1.0-, 1.6-, 2.0-, and 3.0-mm diameter are used with r_C/r_A ranging from 11 to 16. The anode rod extends 16 mm beyond the 3-mm-thick cathode annulus and, for most shots, is tapered to a point over the last 10 mm. The tip of the rod is positioned near the center of a 10-cm-radius, 1-cm-thick hemispherical aluminum shell so that the radiation measurements at different angles are attenuated through 1 cm of aluminum, as shown in Fig. 7. Peak voltages of 5.2–6.3 MV and peak currents of 105–135 kA are measured. The angular distribution of the dose is measured at several angles using an array of five LiF thermoluminescent dosimeters (TLDs) and an array of six silicon pin diodes as shown in Fig. 8. The silicon pin diodes, mounted in lead collimators, provide time histories of the radiation. These radiation diagnostics are described in more detail in [19].

The measured dose increases with angle and the dose at large angles is sufficient to cause saturation effects in the pin diodes [19]. There is no evidence of saturation effects in the smaller signals from the detector at -20°. The time-histories of the radiation at the various TLD locations is inferred by scaling the -20° pin diode pulse shape so that the time-integral is the TLD dose at that location. This scaling is appropriate because the measured TLD dose was observed to scale linearly with the pin diode dose in a previous ASTERIX experiment [17]. Also, for low-dose shots without saturation, no significant differences are observed in the pin diode pulse shapes at different angles.

Calculated and measured dose rates for a 2-mm-diameter tapered rod are compared in Fig. 9. The calculated dose rates are obtained using the measured current (I_T) and voltage (V) waveforms, shown in Fig. 9(a), in conjunction with the power-law fits from the simulations, shown in Fig. 6. The diode voltage is determined by applying an inductive correction to an electrolytic resistive divider located upstream of the diode [20]. This results in a substantial correction of up to 20% to the peak voltage and introduces some uncertainty in the voltage waveform. The current is the average of three B-dot loops located near the diode load. The variation of the individual B-dots from this average is small indicating less than $\pm 5\%$ uncertainty in the current. Both the shapes and magnitudes of the calculated dose rates are in good agreement with the measured dose rates at all five angles [see Fig. 9(b)–(f)].

Fig. 10 shows a comparison of the calculated angular dose distribution with the angular dose distribution measured by the LiF TLDs on ASTERIX for three 2-mm-diameter tapered-anode shots. The peak voltages, currents, and FWHM of the radiation signals are similar for these three shots. The dose distributions for these shots are also similar indicating that the measurements are highly reproducible. The average peak voltage, current, and FWHM of the radiation pulse for these three shots are 6 MV, 110 kA, and 44 ns, respectively (see Fig. 10). The calculated dose is obtained by first multiplying the dose-rate efficiency at the average peak voltage by the current to obtain a peak dose rate. The dose is then calculated by multiplying the peak dose rate by the average FWHM of the radiation pulse. The magnitude and shape of the measured and calculated angular dose distributions agree to within experimental uncertainty. Similar agreement is obtained for a shot with a 1-mm-diameter tapered tungsten rod.

The calculated forward and backward dose-rate efficiencies from the positive-polarity reentrant RPD with 1-mm- and 2-mm-diameter tapered and blunt rods is shown in Fig. 11. In these calculations, photon absorption in the rod at 180° is minimized by using tungsten only for the last 3 mm of the blunt rod and only for the 10-mm taper for the tapered rod. The remainder of the 60-mm-long rod is aluminum. The dose-rate efficiencies are significantly higher for blunt rods than for tapered rods. This indicates that blunt rods take better advantage of the larger electron angles of incidence as the voltage is increased. The dose-rate efficiencies for blunt rods at 10 MV are 15 times larger at 175° than at 5°. The peak dose-rate efficiency at 10 MV is 80 krad/A-s for the 2-mm-diameter blunt rod and 69 krad/A-s for the 1-mm-diameter blunt rod. Therefore, for the reentrant RPD with a 2-mm-diameter [1-mm-diameter] blunt rod with a peak current of 185 kA [208 kA], a dose of 740 rad [720 rad] in a 50-ns FWHM radiation pulse is feasible.

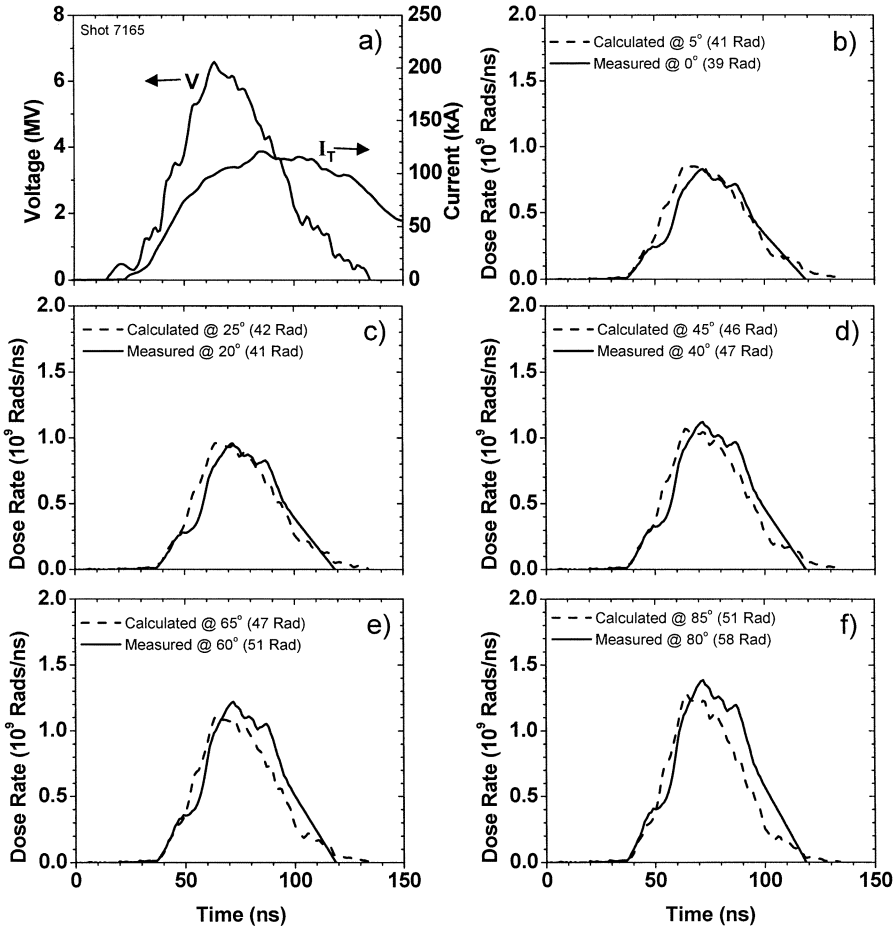

Fig. 9. Comparison of the angular variation of the dose rate from coupled LSP/CYLTRAN simulations with experimentally measured dose rates on ASTERIX for the positive-polarity, reentrant RPD with a 2-mm-diameter tapered anode rod.

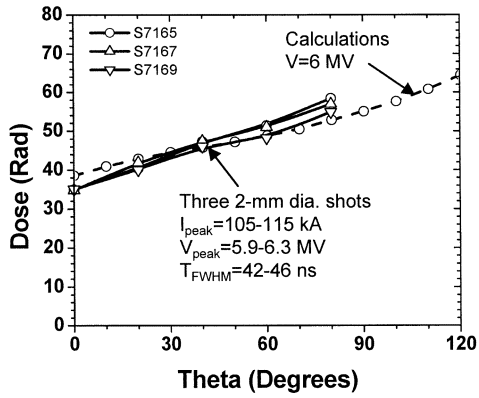

Fig. 10. Comparison of the angular variation of the dose from the coupled LSP/CYLTRAN simulations with the measured angular dose variation from three similarly configured ASTERIX shots.

III. Characterization of Radiation Sources for Voltages up to 10 MV

In the previous section, coupled LSP/CYLTRAN simulations were successfully benchmarked against angular dose measurements in positive polarity. The simulations indicate that the largest dose is toward the generator and not readily available for radiography. The simulations also indicate that the

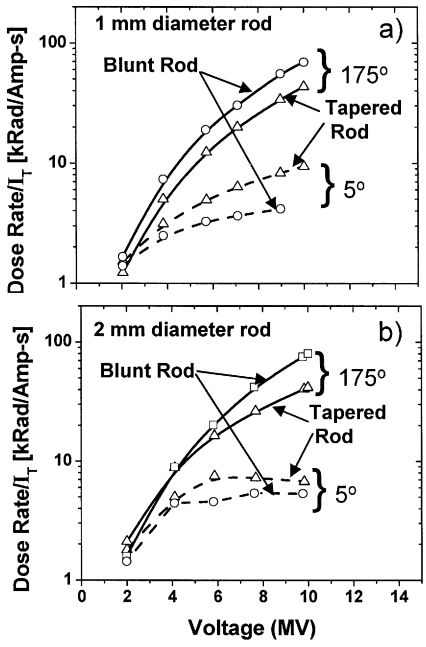

Fig. 11. Forward (5°) and backward (175°) dose-rate efficiencies from the coupled LSP/CYLTRAN simulations for (a) 1-m- and (b) 2-mm-diameter tapered and blunt anode rods.

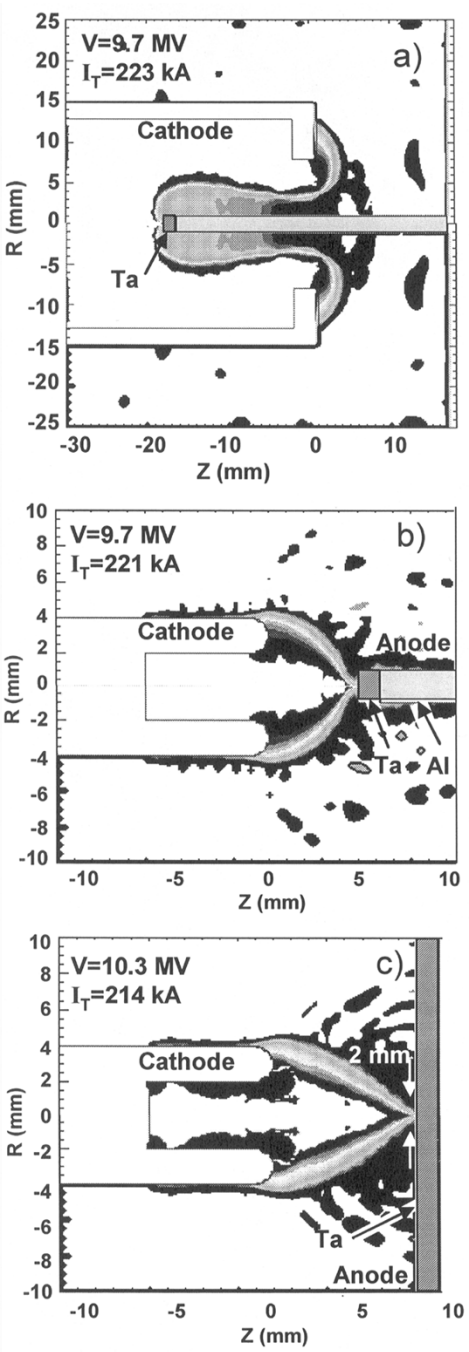

Fig. 12. Current-flow patterns from PIC simulations of negative-polarity SMPD geometries. (a) Reentrant RPD. (b) Nonreentrant RPD. (c) Planar SMPD.

dose is severely limited by a large proton-current fraction. In this section, the on-axis dose and the X-ray spot size from numerical simulations of the negative-polarity SMPD geometries shown in Fig. 1(b)–(d) are compared. All of the geometries analyzed in this section have forward-directed doses comparable to or greater than the peak backward-directed dose in the positive-polarity RPD. This is accomplished by reducing the proton-current fraction and/or decreasing photon absorption. The A-K gap spacing for each geometry is chosen so that each diode operates at about 10 MV and 200 kA.

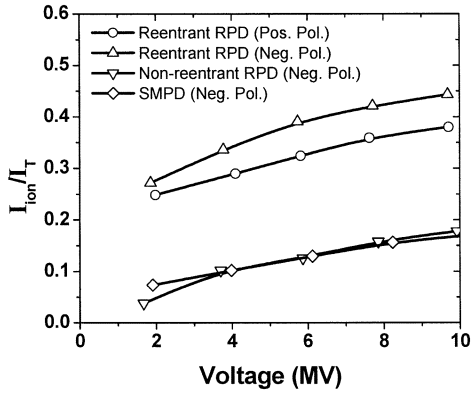

Fig. 13. Proton-current fraction from PIC simulations of the diode geometries depicted in Fig. 1.

The detailed geometry and the current-flow patterns for each of the diodes analyzed in this section are shown in Fig. 12. X-ray emission in the forward direction is filtered through a thickness of aluminum that represents the beam stop and any structures that exist between the source and the object to be radiographed. For the reentrant RPD [Fig. 12(a)], X-rays are attenuated through a total of 44 mm of aluminum. For the nonreentrant RPD [Fig. 12(b)], the X-rays are attenuated through a total of 20 mm of aluminum. For the SMPD [Fig. 12(c)], X-rays are attenuated through a total of 15 mm of aluminum. A tantalum target is used in all of the negative-polarity diode simulations to minimize variations associated with the high-Z target material.

The negative-polarity reentrant geometry [Fig. 12(a)] features a 2-mm-diameter anode rod and a 16-mm-diameter cathode giving an A-K gap of 7 mm. The value of $\mathrm{r_C/r_A}$ was reduced from 11 to 8 to reduce the impedance to nearly 50 Ω. To reduce the absorption of photons in the rod, the anode consists of a 1.3-mm-long tantalum tip on a 34-mm-long aluminum rod. The tantalum thickness is chosen to be about 1/3 of the electron CSDA range at 10 MV [37]. Because the rod extends through the cathode aperture, this geometry has the advantage that the electric field is larger over a large portion of the anode which leads to larger SCL currents than the other two geometries. This allows the diode to pinch at a lower voltage compared with the other two geometries. The simulations show that the electrons are pinched in this geometry for voltages at or above 2 MV. The current-flow pattern at 10 MV shows that current connects with the anode rod over a relatively long length of the rod. Similar flow patterns are observed for voltages at or above 2 MV. Particle plots show that the electron flow is concentrated on the high-Z tip. Therefore, the current flow along the length of the rod is attributed primarily to protons. In this geometry, significant proton current flows from the last 20 mm of the anode rod.

Proton-current fractions for the four diode geometries in Fig. 1 are shown in Fig. 13. The negative-polarity reentrant geometry has the highest proton-current fraction ($\sim 45\%$ at 10 MV) due to the long length from which proton emission occurs. It is even higher than the positive-polarity reentrant case

because r_C/r_A was lowered from 11 to 8 for the negative-polarity reentrant simulation. The forward-directed dose-rate efficiencies for the three negative-polarity diodes and the forward-directed dose-rate efficiency for the positive-polarity reentrant RPD are compared in Fig. 14. The dose-rate efficiency for the negative-polarity reentrant RPD at 10 MV is about 13 times larger than the positive-polarity reentrant RPD. Most of this increase is due to a peak in electron angles of incidence along the axis of the rod that causes a peak in the radiation in the forward direction. The forward-directed dose-rate efficiency for negative-polarity reentrant RPD diode is similar to the backward-directed dose-rate efficiency from the positive polarity reentrant RPD. However, the negative-polarity reentrant RPD diode is configured to extract useful dose out the front of the generator. At 10 MV and 200 kA, the coupled LSP/CYLTRAN simulations predict about 740 rad in a 50-ns FWHM pulse for the negative-polarity reentrant RPD.

The nonreentrant geometry [Fig. 12(b)] uses a 2-mm-diameter anode rod and an 8-mm-diameter hollow cathode. The anode rod consists of a 1.3-mm-long tantalum tip on the end of a 10-mm-long aluminum rod. The distance (D) from the plane of the cathode to the tip of the anode is 5 mm. Because the rod does not extend through the cathode aperture, the electric field in the A-K gap is reduced compared with the reentrant geometry [Fig. 12(a)] and extends over a smaller length of the anode rod. This leads to smaller SCL currents so that a significantly larger voltage is required for pinching. Only electron flows at or above 4 MV are pinched. The critical current for the nonreentrant RPD can be estimated from the cylindrical critical current formula [(2)] with the cathode radius, r_C, replaced with an effective cathode radius that is the distance between the outer edge of the cathode and the center of the anode and given by $r_{Ceff} = (r_C^2 + D^2)^{1/2}$. For the RPD used in the simulation, $r_{Ceff} = 6.5$ mm giving $I_{crit} = 219$ kA at 10 MV which is in good agreement with the simulation. The current-flow pattern at 10 MV [Fig. 12(b)] shows that the majority of the current is concentrated on the end face of the 2-mm-diameter blunt anode rod. Similar flow patterns are observed for voltages at or above 4 MV. Since nearly all of the electrons strike the end of the anode rod, the X-ray spot size is comparable to the diameter of the rod when viewed along the rod axis. For voltages at or below 2 MV, the electron beam is not pinched and the electron flow is distributed over a much longer length of the anode.

Fig. 13 shows that the proton-current fraction at 10 MV for the nonreentrant RPD is reduced to about 17% compared to 40%–45% for the reentrant geometry. This is due to the reduced electric field that is distributed over a smaller region of the anode. The reduction in the proton-current fraction means that approximately 50% more electron current flows to the high-Z target. A comparison of a simulation where proton emission is enabled along the entire length of the rod with a simulation where proton emission is enabled only from the 1.3-mm-long tantalum tip shows virtually identical proton-current fractions. This indicates that nearly all of the protons flow from the final 1.3 mm of the anode. Fig. 14 shows that the increased electron current on to the tantalum target leads to a dose-rate efficiency that is ~ 1.7 times larger at 10 MV than for the negative polarity reentrant RPD. Virtually all of the increase relative to the reentrant geometry can be explained by the increased electron current that results from the decreased proton current. The dose-rate efficiency for the nonreentrant RPD is about 127 kRad/A-s at 10 MV so that a 50-Ω diode would produce about 1270 rad in a 50-ns FWHM pulse.

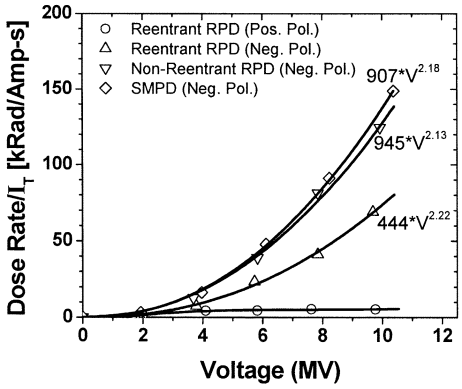

Fig. 14. Dose-rate efficiencies from coupled LSP/CYLTRAN simulations of the diode geometries depicted in Fig. 1.

The planar SMPD [Fig. 12(c)] uses an 8-mm-diameter hollow cathode and a 1.3-mm-thick planar tantalum anode. The anode-cathode gap spacing (d) is defined as the distance from the cathode tip to the anode. The critical current appropriate for the SMPD is the planar critical current formula given by

$$I_{\rm crit}({\rm kA}) = \frac{8.5\alpha(\gamma^2-1)^{1/2}{\rm r_c}}{\rm d}$$

where r_C is the outer radius of the cathode. For the SMPD used in the simulation, $r_C = 4$ mm and $d = 8$ mm so that $I_{crit} = 198$ kA at 10 MV, which is in good agreement with the simulation. The LSP simulations show that electron flows are pinched only for voltages at or above 4 MV. The current-flow pattern at 10 MV [Fig. 12(c)] shows that the majority of the current is concentrated on the tantalum anode within a 2-mm-diameter circle. Similar flow patterns are observed for voltages at or above 4 MV. For voltages at or below 2 MV, the electron beam is not pinched and electrons strike the anode in a larger diameter that is comparable to the cathode diameter. In this voltage range, the X-ray spot size is expected to be much larger than the spot size at higher voltages where the beam is pinched.

Fig. 13 shows that the proton-current fraction at 10 MV for the SMPD is about 17% and is comparable to proton-current fraction for the nonreentrant RPD. The reduction in the proton current fraction is due to the smaller area over which protons are emitted in the SMPD geometry. This means that significantly more electrons flow to the high-Z tantalum target for the SMPD than for the reentrant RPD. Fig. 14 shows that the increased electron flow to the target leads to a dose-rate efficiency that is ~ 1.8 times larger at 10 MV than for the negative polarity reentrant RPD. The 7% difference between the SMPD and the nonreentrant RPD is due to the attenuation of X-rays through an additional 5 mm of aluminum for the RPD. The dose-rate efficiency for the planar SMPD at 10 MV is 137 kRad/A-s so that a 50-Ω diode would produce about 1370 rad in a 50-ns FWHM pulse.

The geometry used in the simulations is similar to recent 4-MV SMPD experiments at AWE [18]. The measurements from six well-aligned shots give a dose of 65 ± 10 rad and a time-integrated spot size of 2.8 ± 0.6 mm. To compare these measurements with simulation, a 50-Ω diode with a peak voltage of 4 MV is assumed with a 50-ns FWHM triangular-shaped radiation pulse. With these assumptions, a dose of 66 rad is predicted from the simulation. The source diameter can be calculated from the simulations by constructing an edge-spread function [38], [39] from the energy-weighted radial distribution of the photons predicted from LSP. This analysis gives a 4.5-mm-diameter spot size at 2 MV that decreases to 1.5 mm at 4 MV. Therefore, considering the variation of spot size with voltage, the simulated dose and spot size are consistent with the recent SMPD measurements.

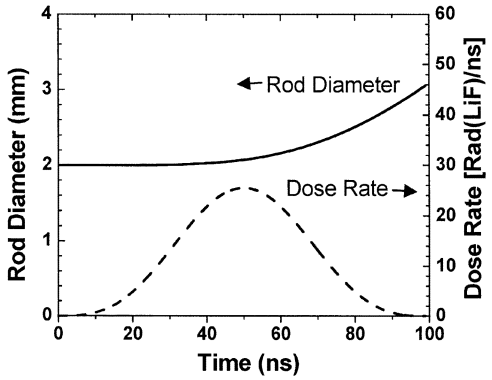

Fig. 15. Time-dependent expansion of the anode rod diameter from a self-similar hydrodynamic expansion model. The time-dependent dose rate used in estimating the radiographic spot size is also shown for timing purposes.

IV. Discussion

Both the negative- and positive-polarity reentrant RPD geometries fall short of the HRF goal of 1000 rad(air). Increases in the dose-rate efficiency for the reentrant geometry can be achieved if the ion-current fraction is reduced. One possible approach is to eliminate protons from the diode and replace them with a heavier ion species. In simulations where protons are replaced with tungsten ions, the ion current fraction is reduced to less than 5%. This results in doubling both the electron current to the high-Z target and the dose-rate efficiency. One possible method for eliminating protons in experiments is to heat the tungsten anode to about 2000 K prior to the shot to drive off hydrocarbon impurities [40]. If the heating techniques are successful, the electron current to the tip of the rod will increase sufficiently to meet the dose requirement for the HRF.

The dose-rate-efficiency from the nonreentrant RPD is sufficient to meet the long-term requirements for the HRF using a spot size given by the 2-mm-rod diameter. However, the spot size may increase due to hydrodynamic expansion driven by electron-beam deposition. To estimate the magnitude of this expansion, a self-similar hydrodynamic model, modified from that developed to study tapered rods used in plasma-filled rod-pinch experiments [38], has been applied to blunt-tip anode rods. In this blunt-tip model, the density of the rod $n(r,t)$ is assumed to be uniform in space with a time-dependent cylindrical radius $R(t)$ so that

$$n(r,t) = \frac{N_0}{\pi R^2(t)} \begin{cases} 1, & 0 \le r \le R(t) \\ 0, & r > R(t) \end{cases} \tag{6}$$

where $N_0 = \rho \pi \mathrm{r}_\mathrm{A}^2 / M$ is the fixed number of particles per length, ρ is the mass density of the rod, and M is the atomic mass. The evolution of $R(t)$ from r_A at $t = 0$ derives from a momentum-balance equation, driven to expand by the plasma kinetic pressure with a temperature determined from a radially integrated energy balance equation [38]. The plasma is heated uniformly by P_abs (W/cm) given by

$$P_\mathrm{abs} = \frac{\eta I_T V (1 - f_\mathrm{Brems})}{\ell_\mathrm{Dep}} \tag{7}$$

where $\eta = 1 - I_\mathrm{ion}/I_T$ is the fraction of the current in electrons, f_Brems is the fraction of the electron energy converted to bremsstrahlung as a function of voltage, and $\ell_\mathrm{Dep} = 1.3$ mm is the length over which the beam deposits energy in the rod. The quantity f_Brems is negligible at low voltage and increases to about 0.3 at 10 MV. The voltage pulse-shape is taken to be sinusoidal with a 10-MV peak and 50-ns quarter period, and the diode impedance is taken to be 50 Ω so that $I_T = V/50$, where V is in volts and I_T is in amperes.

Fig. 15 shows $R(t)$ for a 2-mm-diameter RPD from the self-similar model using these pulse-shapes. Also shown is the dose rate, which is taken from the coupled LSP/CYLTRAN simulations to vary like $945\ I_T V^{2.13}$. The model predicts that the rod plasma expands less than 0.1 mm at the time of peak radiation and $R(t)$ reaches 3 mm by the end of the power pulse. The time-integrated spot size is calculated by weighting the instantaneous density distribution by the dose rate and integrating in time to calculate the point spread function (radial distribution of bremsstrahlung intensity viewed along the rod axis). The point spread is then used to calculate the radiographic line spread function, from which the effective spot size is extracted [38], [39]. This analysis yields a spot size of 2.1 mm for a 2-mm-diameter rod. Therefore, hydrodynamic expansion of a 2-mm-diameter rod does not significantly increase the radiographic spot size. However, rod expansion is expected to be more pronounced for smaller rod diameters. The limitations on dose and spot size due to this expansion will be the subject of future work.

The SMPD simulations indicate that this source will meet or exceed both the dose and spot size requirements for the HRF. However, maintaining a small spot size may be difficult in practice since time-dependent azimuthal asymmetries may cause the pinch location to wander in time. This may be evident in the recent SMPD experiments that show a significant variation in spot size under similar experimental conditions [18]. The nonreentrant RPD geometry might provide a preferred anchor for the focal spot that should alleviate this problem.

The SMPD and nonreentrant RPD simulations predict doses of 1270–1370 rad in the forward direction in a 50-ns FWHM radiation pulse. It is useful to obtain the effective electron angle of incidence on the high-Z target required to make these doses. To

estimate this, a series of ITS simulations were run with the beam energy held constant at 10 MeV and the angle of incidence on the target varied between 0° and 90°. The converter package in these simulations consisted of a 1.3-mm-thick tantalum target and a 20-mm-thick aluminum beam stop. To mimic the large diode electric field, electrons that backscatter from the anode into the diode gap are specularly reflected back into the converter package in the ITS calcuations. The analysis shows that a 16° effective angle of incidence on the target reproduces the forward-directed dose obtained from the LSP/CYLTRAN simulations. The same results are obtained with a uniformly filled cone with a half-angle of 26°. This analysis also shows that the dose increases rapidly as the angle of incidence decreases and as much as 3440 rad could be obtained in the forward direction if all the electrons are normally incident (0°) on the converter. Therefore, substantial increases in the dose can be achieved by decreasing the electron angle of incidence on the target. It may be possible to use the detailed electron orbits from the LSP calculations to reshape the electrodes to reduce the electron angles of incidence on the target and take advantage of the forward-directed radiation patterns. This will be the subject of future work.

Electrode plasma formation and expansion into the anode-cathode gap are not included in these initial calculations. These effects could make significant time-dependent perturbations on the electron orbits, the radiation production efficiency, and the diode impedance. Therefore, while both the SMPD and the nonreentrant negative polarity RPD appear to be viable candidates for meeting the HRF goals, experiments are required to verify their performance and limitations. These experiments should include time-dependent measurements of the expanding anode and cathode plasmas and the X-ray angular dose distribution.

V. Conclusion

The charged-particle dynamics and X-ray production from a positive-polarity RPD has been examined with numerical simulations. The LSP/CYLTRAN simulations agree with both the magnitude and pulse-shape of angular dose-rate measurements from recent experiments on ASTERIX where peak voltages ranged from 5.2 to 6.3 MV. This analysis indicates that, in this voltage range, the dose increases with angle and is a maximum in the direction headed back into the generator. This suggests that, to maximize the extracted dose, future experiments at or above 4 MV should be performed in negative-polarity.

The LSP/CYLTRAN model is used to compare the X-ray dose and spot size from three negative-polarity diode geometries for voltages up to 10 MV; a reentrant RPD, a nonreentrant RPD, and a planar SMPD. For the reentrant RPD, the dose from a 2-mm-diameter anode rod is about 740 rad in a 50-ns FWHM radiation pulse. The proton current is about 45% of the total current, which severely reduces the radiation production efficiency of this diode. For the nonreentrant RPD, the dose from a 2-mm-diameter anode rod is about 1270 rad in a 50-ns FWHM radiation pulse. The increased dose results from a decrease of more than a factor of two in the proton current fraction which significantly increases the electron current to the target. A self-similar model for hydrodynamic expansion of the anode rod indicates that spot-size growth should be minimal for a 2-mm-diameter rod. For the planar self-magnetic-pinched diode, the simulations show that most of the electron-current flow is concentrated within a 2-mm-diameter circle on the anode and the dose is about 1370 rad in a 50-ns FWHM radiation pulse. However, a time-dependent wander in the spot location may lead to an unacceptably large spot size for this diode. In conclusion, numerical simulations show that the nonreentrant RPD and the SMPD are attractive negative-polarity, high-resolution, radiography sources for voltages of up to 10 MV.

Acknowledgment

The authors would like to thank Dr. F. Bayol of the Center d' Etudes de Gramat, Dr. C. Vermare of the Polygone d'Experimentation de Moronvilliers, and the entire ASTERIX experimental team for the high-quality angular dose data. The authors would also like to thank Dr. D. V. Rose, Dr. B. V. Oliver, and Dr. D. R. Welch of Mission Research Corporation, Dr. J. E. Maenchen and Dr. D. C. Rovang of Sandia National Laboratories, Dr. I. Crotch, Dr. D. Short, Dr. M. Sinclair, Dr. J. O'Malley, and Dr. J. Threadgold of the Atomic Weapons Establishment, and Dr. D. D. Hinshelwood and Dr. B. V. Weber of the Naval Research Laboratory for many fruitful discussions related to this work.

References

[1] J. O'Malley, J. Maenchen, and G. Cooperstein, "Status of the diode research programme at AWE," in *Proc. 14th IEEE Int. Pulsed Power Conf.*, Dallas, TX, June 2003, pp. 21–28.

[2] C. Ekdahl, "Modern electron accelerators for radiography," *IEEE Trans. Plasma Sci.*, vol. 30, pp. 254–261, Feb. 2002.

[3] I. D. Smith, P. Corcoran, V. Carboni, V. Bailey, D. L. Johnson, J. Maenchen, I. Molina, R. Carlson, D. Fulton, K. Hahn, J. Smith, D. Droemer, K. Thomas, M. Phillips, S. Croxon, and R. Forgan, "Induction voltage adder architectures and electrical characteristics," in *Proc. 14th IEEE Int. Pulsed Power Conf.*, Dallas, TX, June 2003, pp. 371–378.

[4] M. G. Mazarakis, J. W. Poukey, D. C. Rovang, J. E. Maenchen, S. R. Cordova, P. R. Menge, R. Pepping, L. Bennett, K. Kikkelson, D. L. Smith, J. Hableib, W. A. Stygar, and D. R. Welch, "Pencil-like mm-size electron beams produced with linear inductive voltage adders," *Appl. Phys. Lett.*, vol. 70, no. 7, pp. 832–834, Feb. 1997.

[5] D. Rovang, D. Welch, H. Ives, D. L. Johnson, M. Kincy, B. Lesch, J. Maenchen, P. Menge, I. Molina, B. Oliver, C. Olson, C. Swenson, and D. VanDeVelde, "Status and plans for the next generation magnetically immersed diodes on RITS," in *Proc. 14th Int. Conf. High-Power Particle Beams*, T. A. Mehlhorn and M. A. Sweeney, Eds., Albuquerque, NM, June 2002, pp. 127–130.

[6] D. R. Rovang, S. Cordova, K. Hahn, J. Maenchen, I. Molina, S. Portillo, M. Sceiford, R. Droemer, D. Van de Valde, B. Oliver, D. Rose, D. Welch, and D. Johnson, "Recent progress in the development of immersed diodes," in *Proc. 14th IEEE Int. Pulsed Power Conf.*, Dallas, TX, June 2003, pp. 487–490.

[7] A. R. Birrell, R. D. Edwards, T. J. Goldsack, and M. A. Sinclair, "New developments in paraxial diode technology for focusing intense relativistic electron beams," *IEEE Trans. Plasma Sci.*, vol. 28, pp. 1660–1663, Oct. 2000.

[8] T. J. Goldsack, T. F. Bryant, P. F. Beech, S. G. Clough, G. M. Cooper, R. Davitt, R. D. Edwards, N. Kenna, J. McLean, A. G. Pearce, M. J. Phillips, K. P. Pullinger, D. J. Short, M. A. Sinclair, K. J. Thomas, J. R. Threadgold, M. C. Williamson, and K. Krushelnick, "Multimegavolt multiaxis high-resolution flash X-ray source development for a new hydrodynamics research facility at AWE aldermaston," *IEEE Trans. Plasma Sci.*, vol. 30, pp. 239–253, Feb. 2002.

[9] D. Short, M. Sinclair, D. Rose, and J. Maenchen, "LSP simulations of the paraxial diode and comparisons with experimental data," in *Proc. 14th IEEE Int. Pulsed Power Conf.*, Dallas, TX, June 2003, pp. 744–747.

[10] D. R. Welch, D. V. Rose, B. V. Oliver, E. Shamiloglu, K. Hahn, and J. E. Maenchen, "Transport of a relativistic electron beam in gas and plasma-filled focusing cells for X-ray radiography," *Phys. Plasmas*, to be published.

[11] ——, "Transport of a relativistic electron beam in gas and plasma-filled focusing cells for X-ray radiography," in *Proc. 14th IEEE Int. Pulsed Power Conf.*, Dallas TX, June 15–18, 2003, pp. 495–498.

[12] R. Mahaffey, J. Golden, S. A. Goldstein, and G. Cooperstein, "Intense electron-beam pinch formation and propagation in rod-pinch diodes," *Appl. Phys. Lett.*, vol. 33, no. 9, pp. 795–797, Nov. 1978.

[13] S. B. Swanekamp, R. J. Commisso, G. Cooperstein, P. F. Ottinger, and J. W. Schumer, "Particle-in-cell simulations of high-power cylindrical electron-beam diodes," *Phys. Plasmas*, vol. 7, no. 12, pp. 5214–5222, Dec. 2000.

[14] G. Cooperstein, J. R. Boller, R. J. Commisso, D. D. Hinshelwood, D. Mosher, P. F. Ottinger, J. W. Schumer, S. J. Stephanakis, S. B. Swanekamp, B. V. Weber, and F. C. Young, "Theoretical modeling and experimental characterization of a rod-pinch diode," *Phys. Plasmas*, vol. 8, no. 10, pp. 4618–4636, Oct. 2001.

[15] R. J. Commisso, D. D. Hinshelwood, D. Mosher, P. F. Ottinger, S. J. Stephanakis, S. B. Swanekamp, B. V. Weber, and F. C. Young, "Experimental evaluation of a megavolt rod-pinch diode as a radiography source," *IEEE Trans. Plasma Sci.*, vol. 30, pp. 338–351, Feb. 2002.

[16] P. R. Menge, D. L. Johnson, J. E. Maenchen, D. C. Rovang, B. V. Oliver, D. V. Rose, and D. R. Welch, "Optimization of a rod pinch diode radiography source at 2.3 MV," *Rev. Sci. Instrum.*, vol. 74, no. 8, pp. 3628–3635, Aug. 2003.

[17] F. C. Young, R. J. Commisso, R. J. Allen, D. Mosher, S. B. Swanekamp, G. Cooperstein, F. Bayol, P. Charre, A. Garrigues, C. Gonzales, F. Pompier, and R. Vezinet, "Rod-pinch diode operation at 2 to 4 MV for high-resolution pulsed radiography," *Phys. Plasmas*, vol. 9, no. 11, pp. 4815–4818, Nov. 2002.

[18] I. Crotch, J. Threadgold, M. Sinclair, and A. Pearce, "Self-magnetic pinch diode experiments at AWE," in *Proc. 14th IEEE Int. Pulsed Power Conf.*, Dallas, TX, June 2003, pp. 507–509.

[19] F. C. Young, R. J. Commisso, R. J. Allen, D. Mosher, S. B. Swanekamp, G. Cooperstein, C. Vermare, J. Delvaux, Y. Hordé, E. Merle, R. Nicolas, D. Noré, O. Pierret, Y. R. Rosol, Y. Tailleur, L. Véron, F. Bayol, A. Garrigues, C. Delbos, G. Nicot, B. V. Oliver, D. V. Rose, and J. Maenchen, "Radiographic results for the rod-pinch diode scaled up to 6 MV," in *Proc. 14th IEEE Int. Pulsed Power Conf.*, Dallas, TX, June 2003, pp. 979–982.

[20] R. J. Commisso, F. C. Young, R. J. Allen, D. Mosher, S. B. Swanekamp, G. Cooperstein, F. Bayol, A. Garrigues, C. Delbos, G. Nicot, C. Vermare, J. Delvaux, Y. Hordé, E. Merle, R. Nicolas, D. Noré, O. Pierret, Y. R. Rosol, Y. Tailleur, L. Véron, B. V. Oliver, D. V. Rose, D. Rovang, D. L. Johnson, J. Maenchen, and K. Prestwich, "Overview of the 6-MV, rod-pinch experiment on ASTERIX," in *Proc. 14th IEEE Int. Pulsed Power Conf.*, Dallas, TX, June 15–18, 2003, pp. 479–482.

[21] S. B. Swanekamp, R. J. Commisso, R. J. Allen, D. Mosher, G. Cooperstein, F. C. Young, C. Vermare, J. Delvaux, Y. Hordé, E. Merle, R. Nicolas, D. Noré, O. Pierret, Y. R. Rosol, Y. Tailleur, L. Véron, F. Bayol, A. Garrigues, C. Delbos, G. Nicot, B. V. Oliver, D. V. Rose, and J. Maenchen, "Angular dose variations from 4- to 6-MV rod-pinch experiments on the ASTERIX pulsed-power generator," in *Proc. 14th IEEE Int. Pulsed Power Conf.*, Dallas, TX, June 2003, pp. 483–486.

[22] G. Cooperstein, S. B. Swanekamp, J. W. Schumer, P. F. Ottinger, and R. J. Commisso, "Considerations of rod-pinch diode operation in negative polarity for radiography," in *Proc. 14th IEEE Int. Pulsed Power Conf.*, Dallas, TX, June 2003, pp. 975–978.

[23] D. R. Welch, D. V. Rose, B. V. Oliver, and R. E. Clark, "Simulation techniques for heavy ion fusion chamber transport," in *Nucl. Meth. Phys. Res. A*, vol. 464, 2001, pp. 134–139.

[24] D. V. Rose, D. R. Welch, B. V. Oliver, R. E. Clark, D. L. Johnson, J. E. Maenchen, P. R. Menge, C. L. Olson, and D. C. Rovang, "Coupled particle-in-cell and Monte Carlo transport modeling of intense radiographic sources," *J. Appl. Phys.*, vol. 91, no. 5, pp. 3328–3335, Mar. 2002.

[25] J. A. Halbleib, R. P. Kensek, G. D. Valdez, S. M. Seltzer, and M. J. Berger, "ITS: The integrated TIGER series of electron/photon transport codes-Version 3.0," *IEEE Trans. Nucl. Sci.*, vol. 41, pp. 1025–1030, Aug. 1992.

[26] I. Langmuir and K. Blodgett, "Currents limited by space-charge between coaxial cylinders," *Phys. Rev.*, ser. 2, vol. 22, pp. 347–356, Oct. 1923.

[27] I. Langmuir, "Interaction of electron and positive ion space charge in cathode sheaths," *Phys. Rev.*, vol. 33, pp. 954–989, June 1929.

[28] B. V. Oliver, T. C. Genoni, D. V. Rose, and D. R. Welch, "The impedance characteristics of a rod-pinch diode," in *Proc. 13th Int. Pulsed Power Conf.*, Las Vegas, NV, June 2001, pp. 458–461.

[29] P. F. Ottinger, J. W. Schumer, S. Strasburg, S. B. Swanekamp, and B. V. Oliver, "Non-laminar flow model for the impedance of a rod-pinch diode," in *Proc. 14th Int. Conf. High-Power Particle Beams*, Albuquerque, NM, June 2002, pp. 187–190.

[30] ——, "Vlasov model for the impedance of a rod-pinch diode," in *Proc. 14th IEEE Int. Pulsed Power Conf.*, Dallas, TX, June 2003, pp. 987–990.

[31] G. Cooperstein, P. F. Ottinger, J. W. Schumer, S. B. Swanekamp, R. J. Allen, R. J. Commisso, D. D. Hinshelwood, D. Mosher, S. J. Stephanakis, B. V. Weber, and F. C. Young, "The influence of anode-plasma location on total current in self-magnetically-limited electron-beam diodes," in *Proc. 14th Int. Conf. High-Power Particle Beams*, Albuquerque, NM, June 2002, pp. 215–219.

[32] S. A. Goldstein and R. Lee, "Ion-induced pinch and enhancement of ion current by pinched electron flow in relativistic diodes," *Phys. Rev. Lett.*, vol. 35, no. 16, pp. 1079–1082, Oct. 1975.

[33] K. D. Bergeron, "Two-species flow in relativistic diodes near the critical field for magnetic insulation," *Appl. Phys. Lett.*, vol. 28, no. 6, pp. 306–308, Mar. 1976.

[34] D. W. Swain, S. A. Goldstein, J. G. Kelly, and G. R. Hadley, "Observation of anode ions associated with pinching in a relativistic electron beam diode," *J. Appl. Phys.*, vol. 46, no. 10, pp. 4604–4605, Oct. 1975.

[35] D. Mosher, R. J. Allen, R. J. Commisso, S. B. Swanekamp, F. C. Young, G. Cooperstein, C. Vermare, J. Delvaux, Y. Hordé, E. Merle, R. Nicolas, D. Noré, O. Pierret, Y. R. Rosol, Y. Tailleur, L. Véron, F. Bayol, A. Garrigues, C. Delbos, G. Nicot, B. Oliver, D. V. Rose, D. Rovang, and J. Maenchen, "Characterization of composite rod-pinch-diode radiographic sources at 5 to 6 MV on ASTERIX," in *Proc. 14th IEEE Int. Pulsed Power Conf.*, Dallas, TX, June 2003, pp. 983–986.

[36] NIST X-Ray Coefficients [Online]. Available: http://physics.nist.gov/PhysRefData/XrayMassCoef.

[37] NIST Electron Range Tables [Online]. Available: http://physics.nist.gov/PhysRefData/Star/Text/ESTAR.html

[38] D. Mosher, J. W. Schumer, B. V. Weber, and D. Ponce, "Electrode-Expansion MHD in a plasma-filled rod pinch," in *Proc. 14th IEEE Int. Pulsed Power Conf.*, Dallas, TX, June 2003, pp. 503–506.

[39] J. C. Dainty and R. Shaw, *Image Science*. New York: Academic, 1974, p. 232.

[40] B. V. Weber, R. J. Allen, B. G. Moosman, S. J. Stephanakis, F. C. Young, N. R. Pereira, and J. R. Goyer, "Improved bremsstrahlung from diodes with pulse-heated tantalum anodes," *IEEE Trans. Plasma Sci.*, vol. 30, pp. 1806–1815, Oct. 2002.

Stephen B. Swanekamp was born in Bethesda, MD, on November 15, 1959. He received the B.S. degree in electrical engineering and mathematics from the University of Maryland, College Park, in 1984 and the M.S. and Ph.D. degrees in nuclear engineering from the University of Michigan, Ann Arbor, in 1990.

Between 1990 and 1993, he was a National Research Council Research Associate with the Pulsed Power Physics Branch, Plasma Physics Division, Naval Research Laboratory (NRL), Washington, DC. Since 1993, he has been a contract employee at NRL. He is currently the Principal Investigator for pulsed-power research efforts at Jaycor, Inc., McLean, VA. His current research interests include the physics of long conduction time plasma opening switches and high-power electron beam diodes.

Gerald Cooperstein received the B.S. degree in physics and the Ph.D. degree in experimental high-energy physics from the Massachusetts Institute of Technology, Cambridge, in 1963 and 1968, respectively.

His first two positions were with EG&G and Ion Physics Corporation, where he worked on generating intense electron beams for simulating nuclear weapon effects. He joined the Naval Research Laboratory (NRL), Washington, DC, as a Section Head in the Plasma Physics Division in 1971, where he was responsible for performing similar research on the newly developed Gamble high-voltage, pulsed power generator. He is currently head of the NRL's Pulsed Power Physics Branch, which is responsible for research into the technology and applications of pulsed power science. In 1992, he served as Co-Chairman of BEAMS'92, the 9th International Conference on High-Power Particle Beams, Washington, DC. In 1995, he served as Technical Program Chairman of the 10th IEEE International Pulsed Power Conference, Albuquerque, NM, and, in 1997, as Chairman of the 11th IEEE International Pulsed Power Conference, Baltimore, MD. In addition, he served as Co-Editor of the published proceedings for all three conferences. He has co-authored over 150 publications and professional society presentations on the subjects of high-voltage pulsed-power and intense electron- and ion-beam generation.

Dr. Cooperstein was elected a Fellow of the American Physical Society in 1987. He was a Guest Editor of two special issues of the IEEE TRANSACTIONS ON PLASMA SCIENCE, one devoted to plasma opening switches in December 1987 and another devoted to pulsed-power science and technology in April 1997. The pulsed-power community recognized him in 1999 with the IEEE Peter Haas Pulsed Power Award.

Joseph W. Schumer was born in Cape Girardeau, MO, on February 9, 1969. He received the B.S. degree in nuclear engineering from the University of Missouri, Rolla, in 1992, and the M.S. and Ph.D. degrees in nuclear engineering from the University of Michigan, Ann Arbor, in 1994 and 1997, respectively.

Between 1997 and 1999, he was a National Research Council Research Associate with the Pulsed Power Branch, Plasma Physics Division, Naval Research Laboratory (NRL), Washington, DC. Between December 1999 and July 2000, he was a Research Scientist at NRL with Jaycor, Inc., McLean, VA, and began as an NRL employee in August 2000. His current research interests include the development of improved numerical models for collisionless and collisional plasmas and the physics of high-energy electron-beam transport.

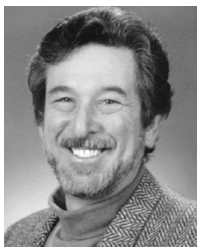

David Mosher was born on September 28, 1942. He received the B.S. in physics from Queens College, New York, in 1963, and the Ph.D. degree in astrophysical sciences from Princeton University, Princeton, NJ, in 1968.

Following a Post-Doctoral Fellowship at Los Alamos National Laboratory, Los Alamos, NM, and an Assistant Professorship at The Ohio State University, Columbus, he joined the Plasma Physics Division, Naval Research Laboratory, Washington, DC, in 1972. Since that time, he has carried out experimental and theoretical research using terawatt-level pulsed-electrical power to create high-energy-density, X-radiating Z-pinch plasmas, intense ion beams, and intense electron beams, to manipulate, focus, and transport such radiations, and to study their interactions with matter.

Dr. Mosher is a Fellow of the American Physical Society and a Member of Sigma Xi.

F. C. Young received the Ph.D. degree from the University of Maryland, College Park, in 1962.

He conducted experimental nuclear physics research for ten years. In 1972, he joined the Naval Research Laboratory (NRL), Washington, DC, and began applying his expertise with radiation measurements to a variety of high-power pulsed-plasma sources. His studies have included hot electrons from laser-plasma interactions, neutrons and energetic ions from exploding wires, X-rays from imploding Z-pinch plasmas, novel diagnostics for intense energetic ion beams, enhanced stopping of MeV ions in hot dense plasmas, and population inversion of a photopumped Z-pinch plasma for soft X-ray lasing. He retired from the NRL in 1997, but continues to work part time as a consultant.

Paul F. Ottinger (SM'01) was born in Philadelphia, PA, in 1948. He received the B.A. degree in physics from the University of Pennsylvania, Philadelphia, in 1970 and the M.S. and Ph.D. degrees in theoretical plasma physics from the University of Maryland, College Park, in 1974 and 1977, respectively.

Since 1985, he has been with the Naval Research Laboratory (NRL), Washington, DC, as the Head of the Theory and Analysis Section, Pulsed Power Physics Branch. Before joining the NRL, he was a National Research Council Associate and worked as a Senior Research Scientist in private industry for Jaycor, Inc., McLean, VA. During his career, he has developed expertise in the specialized areas of intense particle beams, fast-opening plasma switches, diode physics, and plasma radiation sources. In particular, his research has concentrated on the areas of ion-beam generation, transport, and stability.

Dr. Ottiger is a Fellow of the American Physical Society (APS) and the recipient of the 1992 IEEE Plasma Science and Applications Award.

Robert J. Commisso was born in Queens, NY. He received the B.S. degree in physics from the Lowell Technological Institute (now the University of Massachusetts at Lowell), Lowell, MA, in 1968 and the Ph.D. degree in physics from the University of Maryland, College Park, in 1976, where he studied plasma physics.

From 1976 to 1980, he was a Staff Member at the Los Alamos National Laboratory, Los Alamos, NM, where he worked on controlled fusion research. In 1980, he joined Jaycor, Inc., McLean, VA, as a Senior Research Scientist, developing novel opening switch concepts at the Naval Research Laboratory (NRL), Washington, DC. He joined the NRL as Head of the Pulsed Power Staff, Plasma Technology Branch, in 1984. He is currently Head of the Advanced Systems Section, Pulsed Power Physics Branch, a Co-Principal Investigator for DTRA pulsed-power development, and serves as a Technical Advisor to DTRA. His research interests include plasma opening switches, Z-pinches, production of intense X-ray radiation for various applications, and advanced pulsed power development.